NANO LETTERS

Letter

pubs.acs.org/NanoLett

Measuring Uptake Dynamics of Multiple Identifiable Carbon Nanotube Species via High-Speed Confocal Raman Imaging of Live Cells

Jeon Woong Kang,[†] Freddy T. Nguyen,[†,‡] Niyom Lue,[†] Ramachandra R. Dasari,[†] and Daniel A. Heller*[,§]

[†]Laser Biomedical Research Center, G. R. Harrison Spectroscopy Laboratory, Massachusetts Institute of Technology, Cambridge, Massachusetts 02139, United States

[‡]College of Medicine, University of Illinois at Urbana−Champaign, Urbana, Illinois 61801, United States

[§]Molecular Pharmacology and Chemistry Program, Memorial Sloan-Kettering Cancer Center, New York, New York 10065, United States

Supporting Information

ABSTRACT: Carbon nanotube uptake was measured via high-speed confocal Raman imaging in live cells. Spatial and temporal tracking of two cell-intrinsic and nine nanotube-derived Raman bands was conducted simultaneously in RAW 264.7 macrophages. Movies resolved single (*n*, *m*) species, defects, and aggregation states of nanotubes transiently as well as the cell position, denoted by lipid and protein signals. This work portends the real-time molecular imaging of live cells and tissues using Raman spectroscopy, affording multiplexing and complete photostability.

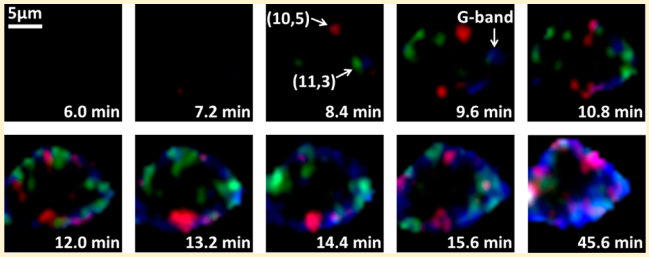

KEYWORDS: *Single-walled carbon nanotube, Raman spectroscopy, resonance Raman scattering, Raman microscopy, intracellular trafficking, molecular probe*

Raman scattering has been employed substantially in recent years for biomedical applications. The high signal amplification of surface-enhanced Raman scattering (SERS)[1] has generated excitement for molecular sensing and imaging studies in live cells. Single-walled carbon nanotubes (SWNTs) are a class of materials with extremely high Raman cross sections due to resonance enhancement, which results in high signals without the need for surface plasmon-generating metals such as silver and gold.[2] The resonance enhancement of SWNTs stems from the optical absorption bands caused by the Van Hove singularities of the 1D electronic structure of the nanotubes.

Single-walled carbon nanotubes have shown promise in biomedical applications such as drug and nucleic acid delivery,[3,4] optical[5,6] and electronic[7] sensors. Carbon nanotube-based probes[8−11] benefit from the large aspect ratio and surface area, allowing for multivalent binding sites.[12] Signals are optically stable and quantitative and can often be employed for use in the near-infrared "tissue-transparent" window. With over 50 different species, each possessing unique optical and electronic properties, labeling applications could potentially take advantage of the large number of individually addressable probes. The different structures of single-walled carbon nanotubes are denoted by two indices, *n* and *m*, that correspond to the two lattice vectors on a sheet of graphene. Each (*n*, *m*) designation represents a particular nanotube species with its own unique electronic and optical properties.

Carbon nanotubes produce Raman scattering from several vibrational modes,[13] such as the tangential mode of graphene (G band) at ∼1590 cm^{-1} and radial breathing modes (RBMs) in the vicinity of 120−350 cm^{-1} for nanotubes of between 0.7 and 2 nm in diameter as well as intermediate-frequency modes[14,15] (IFM) that appear between the RBM and G-peak regions. The unique Raman shifts of the RBMs and IFMs are highly dependent on the nanotube graphitic species, allowing the identification of the nanotube (*n*, *m*) species present. The RBM frequencies, caused by the axial vibration of the nanotube's circumference, relate to nanotube diameter with the relation $\omega_{RBM} = (228/d_t) + 16$ cm^{-1}.[16] The IFMs have not been as extensively studied as the other modes, but certain modes with frequencies of between 380 and 650 cm^{-1} have been assigned to nanotube (*n*, *m*) species or families of species.[15] Some IFMs exhibit stepwise dispersion, changing in frequency upon excitation at different laser energies, and other modes are nondispersive.[14] Other information gained from carbon nanotube samples by Raman spectra includes the presence of metallic nanotubes via the Breit−Wigner−Fano (BWF) line shape of the tangential mode,[2] the presence of sp^3 carbon defects via the 1297 cm^{-1} disorder mode (D peak),[2] and the presence of van der Waals contact in the RBMs. For

Received: August 10, 2012
Revised: October 19, 2012

   dx.doi.org/10.1021/nl302991y | *Nano Lett.* XXXX, XXX, XXX−XXX

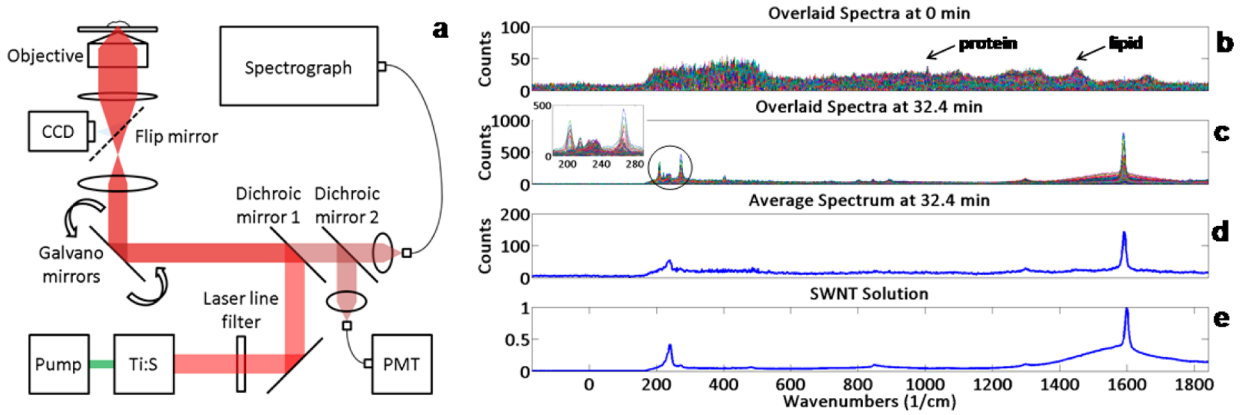

Figure 1. (a) Schematic of a high-speed confocal Raman imaging microscope employing galvano mirrors for raster scanning the laser beam across the specimen. (b) Overlaid Raman spectra of one full raster scan of a cell just after introducing carbon nanotube-containing media ($T = 0$) showing cellular lipid (1450 cm^{-1}) and protein (1004 cm^{-1}) Raman features but no carbon nanotube features. (c) Overlaid Raman spectra of one full raster scan of the same cell 32.4 min after the introduction of nanotube-containing media showing strong nanotube RBM, tangential, IFM, and disorder modes. The cellular signal is present but dwarfed by the nanotube modes. (d) Aggregate Raman spectrum of nanotubes in the cell showing convoluted Raman peaks. (e) Spectrum of the $ss(AT)_{15}$ oligonucleotide-suspended carbon nanotube sample used in this study.

instance, at 785 nm excitation, the (10, 2) nanotube at 267 cm^{-1} comes into resonance upon such contact, denoting aggregation or "bundling."[17]

Confocal Raman mapping of biological tissues and single cells has been developed and employed for diagnostic applications.[18] Raman spectroscopy can distinguish macromolecules as well as structural features such as organelles based on their characteristic Raman spectra.[19,20] Raman modes visible in single cells include lipids, proteins, and nucleic acids. Recently, the G. R. Harrison Spectroscopy Laboratory developed a high-speed confocal Raman microscopy system using galvano mirrors instead of mechanical stage movement, used in most commercial systems.[19] This high-throughput system has greatly increased the image acquisition speed, allowing the high-resolution mapping of a single cell in under a minute (30 pixels × 30 pixels over a 17 μm × 17 μm field of view). This development allows for transient imaging of live cells and the tracking of nanomaterials within them.

Herein, we observe the real-time uptake of individual single-walled carbon nanotube species into live macrophages via transient spatial Raman mapping. Signals from DNA-encapsulated carbon nanotubes[21] and lipid and protein signatures of the cells are measured concurrently. The uptake of several individual carbon nanotubes is observed via strong Raman scattering of radial breathing mode (RBM) and intermediate frequency mode (IFM) features. The nanotubes are tracked spatially and temporally via rapid, continuous Raman spectral mapping of the cells with a frame rate approaching 1 map/min. The nanotube signals and cell-intrinsic lipid and protein signals are acquired concomitantly, allowing the localization of the nanotubes with respect to the cell position. Early in the experiments, RBM signatures of individual nanotubes account for the majority of the nanotube signal. After 15 min, however, the aggregate G-band signal becomes dominant, as multiple nanotube species out of RBM resonance flood the cells. This work demonstrates the real-time tracking of multiple, distinguishable, nanoparticles in cells via Raman mapping for applications in molecular probes, surgical markers, and contrast agents.

A home-built confocal Raman microscopy system (Figure 1a) was described previously.[19] Briefly, a 785 nm wavelength Ti:sapphire laser (3900S, Spectra-Physics) was used for the excitation. High-speed *XY* scanning was done by galvano mirrors (CT-6210, Cambridge Technology). A 1.2 NA water immersion objective lens (Olympus UPLSAPO60XWIR 60X/1.20) was used both to focus the laser onto a cell and to collect the backscattered light. The backscattered Raman light from the sample passes through two dichroic mirrors (DM1 = Semrock LPD01-785RU-25, DM2 = Semrock LPD01-785RU-25 × 36 × 1.1) and was collected by a multimode fiber (Thorlabs M14L01). The collected signal was delivered to a spectrograph (Holospec f/1.8i, Kaiser Optical Systems) and detected by a TE-cooled, back-illuminated, deep depleted CCD (PIXIS: 100BR_eXcelon, Princeton Instruments). The rejected Rayleigh light from the second dichroic mirror (DM2) is collected by a single-mode fiber (Thorlabs P1-780A-FC-1) and delivered to a photomultiplier tube (PMT, H9656-20, Hamamatsu) that is amplified by a PMT controller (C7169, Hamamatsu). This provides an exactly coregistered confocal reflectance image that guides Raman mapping for an optimal field of view. Labview 8.6 software (National Instruments) and a data acquisition board (PCI-6251, National Instruments) are used to control the devices.

Single-walled carbon nanotubes synthesized by the HiPCO process[22] (Unidym) were suspended by $ss(AT)_{15}$ oligonucleotide by sonicating with a probe tip (Sonics & Materials) at 10 W for 10 min in a water bath and centrifuged at 20 000*g* for 90 min. This produced DNA-encapsulated nanotubes demonstrated to be biocompatible and stable in aqueous solution without the need for a surfactant.[8,21] Mouse leukemic monocyte macrophage cells (RAW 264.7) were cultured in Dulbecco's Modified Eagle's Medium (DMEM) with 10% fetal bovine serum (FBS) and 1% antibiotics. Macrophages were plated onto 60 mm Petri dishes modified to incorporate a quartz bottom. The cells were allowed to adhere to the quartz-bottomed plates for at least 48 hours before imaging. Immediately prior to imaging, the cell media was replaced with media containing 1 mg/L DNA-encapsulated nanotubes. The near-infrared laser wavelength and excitation power of 60 mW ensured that the cells remain viable during the course of the measurement. The mapping process involved the rapid scanning of a 17 μm × 17 μm area, acquiring 900 (30 × 30) spectra, each with an integration time of 50 ms. Because of the time delay between each acquisition, the effective acquisition

dx.doi.org/10.1021/nl302991y | *Nano Lett.* XXXX, XXX, XXX−XXX

time was 75 ms and the total acquisition time per image was 68 s. With a minimal interval between frames, the experiments produced 36 000 (30 × 30 × 40) Raman spectra.

Initial Raman measurements of the cell exhibited only cell-intrinsic Raman features, including lipids (1450 cm^{-1}) and proteins (1004 cm^{-1}) (Figure 1b). Five minutes after the injection of the nanotubes, they began to enter the cell. Although typical signal strengths of cellular lipids and proteins were 7−10 times that of the noise, nanotube RBM peaks reached 150 times and the G band reached 500 times. In the initial minutes of the experiment, carbon nanotube signals often appeared to favor RBMs, often exhibiting a higher signal than the G-band in some spectra. Notably, a sole RBM or IFM peak was often recorded in a single spectrum, denoting the presence of only one visible nanotube species at a particular location (Figure 1c). The disorder mode and BWF line shape were present in the cell but not in all spectra containing nanotube species, suggesting that metallic nanotubes and those with defects were spatially discerned within the cells. An aggregate spectrum of the entire region at the same time point shows few of the individual features seen in the spatially resolved spectra (Figure 1d), instead resembling a spectrum of the original DNA−nanotube stock solution (Figure 1e).

All Raman spectra were fit with a linear combination of normalized basis Lorentzian spectra with non-negative restriction. Basis spectra were generated with known peak centers from the literature. To avoid data overfitting, the process was carefully monitored by restricting the fitting coefficient to non-negative values. As a result, we acquired 36 000 coefficients for each basis spectrum. These coefficients were used to construct image series from spatial (30 × 30) and temporal (40 temporal points) coordinates. The data analysis software was developed in-house using MATLAB. The experiments detected RBM peaks at 203, 215, 225, 233, and 267 cm^{-1} corresponding to the (13, 3), (9, 7), (10, 5), (11, 3), and (10, 2) species/bundling, respectively. The IFM modes at 401 and 844 cm^{-1}, disorder mode at 1297 cm^{-1}, and G-band at 1590 cm^{-1} were also detected within cells and included in the fitting process (Figure 2a). The fitting coefficient of each basis spectrum represents the relative strength of each component and was used to reconstruct images. Figure 2b shows the spatially mapped intensity of each fitted nanotube-based mode as well as the 1450 cm^{-1} lipid and 1004 cm^{-1} protein peaks at 32.4 min during the experiment. The cellular lipid signal was used to define the cell location and delineate cell boundaries. This peak was used to determine that a particular feature, present in the upper-right corner of the G band (203, 267, 401, and 1297 cm^{-1} mode images), was in fact not within the cell membrane and likely adsorbed to the quartz substrate. It is reasoned that the spot denotes a carbon nanotube aggregate (bundle) due to the presence of a large 267 cm^{-1} (bundling) peak.

The dynamics of the macrophage uptake of nanotubes were measured by quantifying cell-localized nanotube Raman signals over the course of the experiment. A plot of the average intensity of each Raman feature over time within the confines of the cell shows the relative accumulation of each nanotube species within the macrophage (Figure 3a, S1). Although the G-band signal exhibited an increasing trend through much of the course of the experiment, the RBM and IFM features did not increase at the same rate. The relative G-band signal in the cell, normalized to the total nanotube-derived signal, is plotted versus time in Figure 3b. In the first few minutes of nanotube

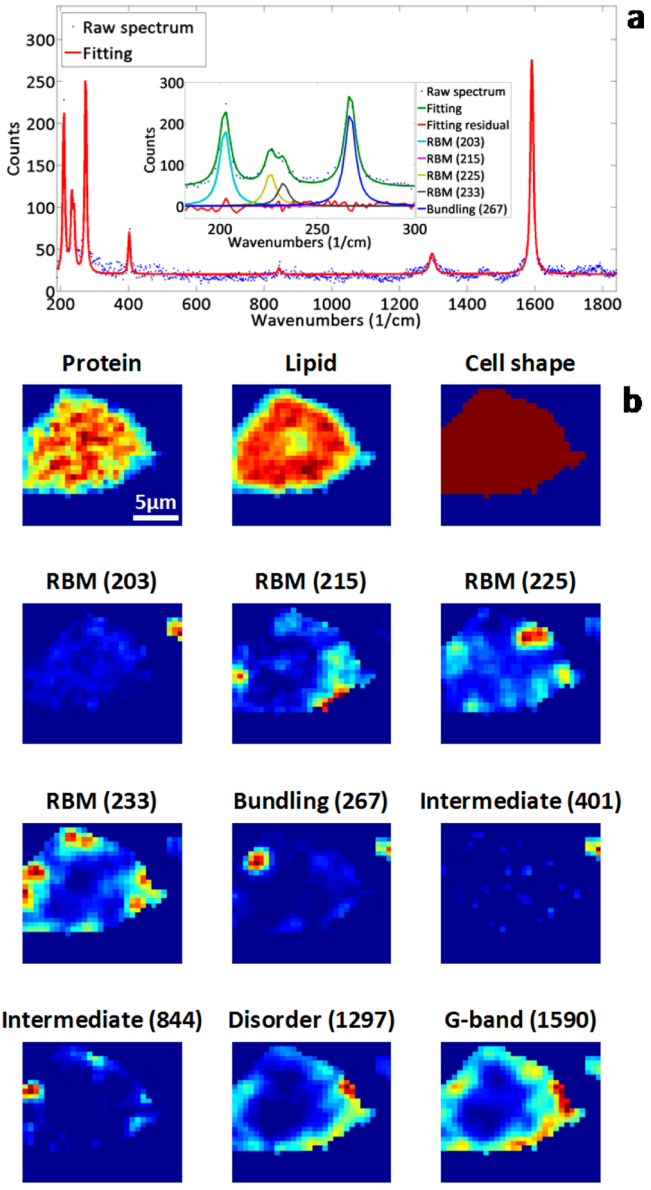

Figure 2. (a) Example Raman spectrum of multiple clearly differentiable nanotube RBMs with intensities approaching that of the G band. The spectrum was spectrally deconvoluted to quantify the RBM, IFM, disorder, and G band. (Inset) Magnified RBM region showing deconvoluted peaks. (b) Raman intensity maps of a single RAW 264.7 macrophage 32.4 min after introducing nanotubes. Each map was compiled using the intensity of a single Raman mode from an endogenous cell-based peak (lipids and proteins) or a nanotube-derived peak (RBMs, IFMs, disorder, and G band). The cell shape was derived from the lipid peak.

incubation, the G-band signal accounted for a small proportion of the total Raman signal in the macrophage. After approximately 14 min, the G-band signal intensity equaled the aggregate RBM signal. The inverse effect is apparent by plotting the normalized RBM signal versus time. A control experiment performed in the absence of cells showed no such relative increase in the G band (Figure S2).

We attribute the apparent increase in the G band to two photophysical factors: the RBMs do not have the same resonances as the G band, and the bandwidths of the resonance windows differ.[23] Early in the accumulation process, the nanotubes are spatially separated within the cell so that each

dx.doi.org/10.1021/nl302991y | Nano Lett. XXXX, XXX, XXX−XXX

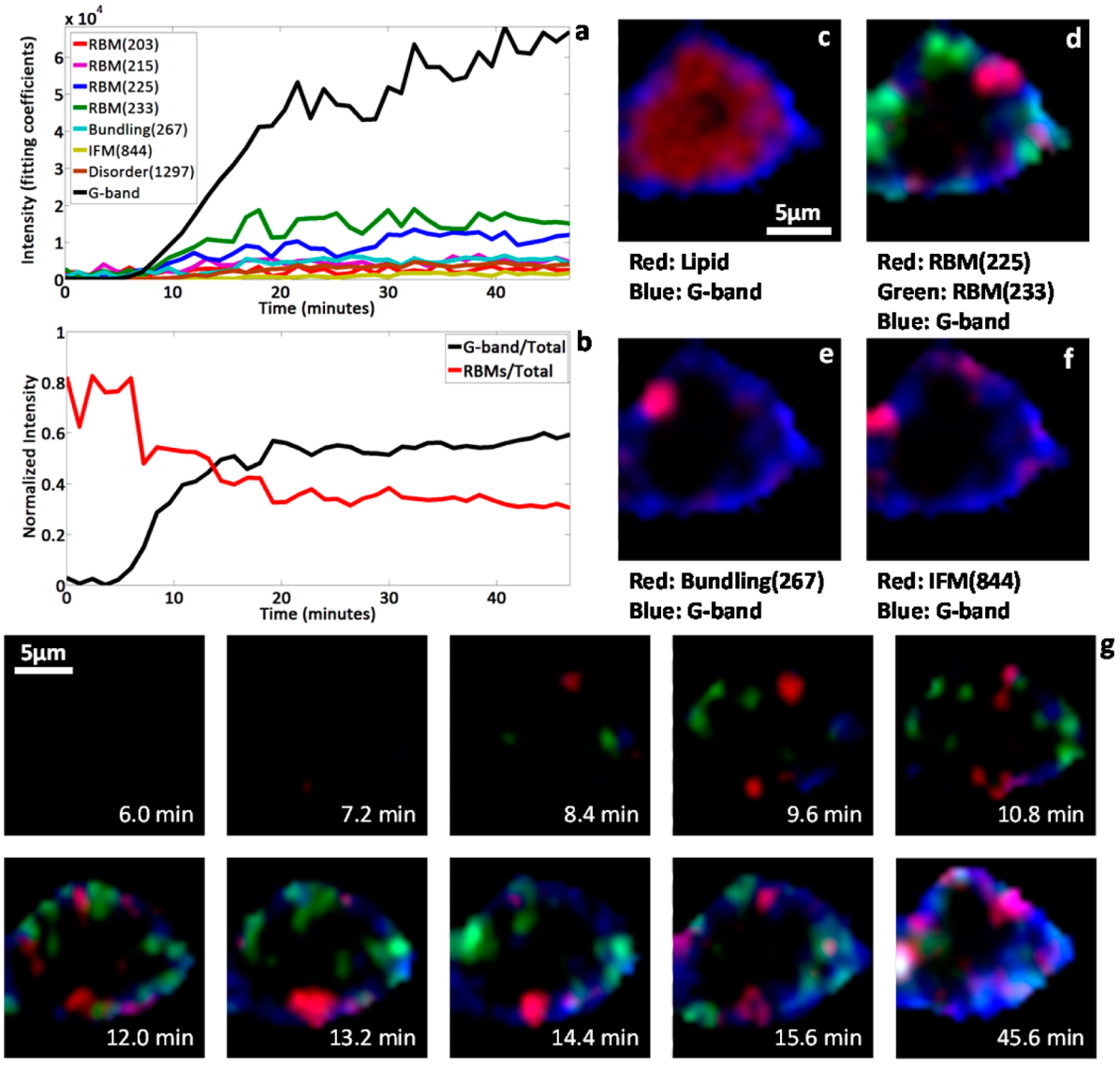

Figure 3. (a) Uptake of several carbon nanotube Raman modes measured within a live macrophage. (b) Relative G-band signal, normalized to the total nanotube-derived Raman signal in the cell, plotted over time. The G band represents an increasing proportion of total nanotube signal in the cell. The inverse is seen by plotting the RBM signal versus the total signal. (c–f) Single frames taken at 32.4 min from movies (in Supporting Information) showing cell-intrinsic features and nanotube-based features within the confines of the cell. (g) Time series of movie frames from Movie M2 showing the uptake of two nanotube species, as defined by their RBMs, and the G band. Earlier images show few G-band features with respect to the total Raman signal, but later images exhibit the opposite.

spectrum is acquired while the laser is focused on one or a few nanotubes. The spectra at these time points often contain a single RBM peak. Individual RBM modes excited on resonance are relatively intense compared to the G band. The convolution of the spectrum increases as multiple nanotube species begin to accumulate at the same relative location, resulting in spectra containing species whose RBMs are weak or absent but whose tangential modes still contribute to the aggregate G-band signal because of its relatively large resonance window.

Movies (Supporting Information) of endogenous and exogenous features were constructed from nanotube-derived and cell-intrinsic Raman modes (Figure 3c–g). A movie showing the carbon nanotube G band and the cellular lipid peak (Movie M1) together demonstrate the transient encroachment of the nanotubes into the cellular space over a time frame of several minutes (still image at 32.4 min shown in Figure 3c). The transient uptake of three Raman features, including two RBMs and the G band, are shown in Movie M2 (corresponding still image at 32.4 min shown in Figure 3d and time series in Figure 3g). Note that the progression shows individual RBM features present in the cell soon after its exposure to nanotubes. The RBM signals outweigh the G-band signals, especially at the beginning of cell uptake. Later in the movie, the G band becomes more prominent. Bundled nanotubes, denoted by the 267 cm^{-1} peak (Movie M3, Figure 3e), were detected with a low rate of incidence, corresponding to the overall low intensity of the 267 cm^{-1} mode in the original nanotube sample (Figure 1). The 844 cm^{-1} IFM (Movie M4, Figure 3f) was also easily tracked with respect to the G band, showing few species present.

We have demonstrated the first transient cellular uptake imaging of nanomaterials and the first transient imaging of carbon nanotubes with the ability to distinguish multiple pristine carbon nanotube species. Using our unique instru-

dx.doi.org/10.1021/nl302991y | *Nano Lett.* XXXX, XXX, XXX–XXX

mentation, we acquired movies of both nanotube-based and cell-intrinsic Raman signals. This data allowed the cellular transient tracking of four nanotube (n, m) species by RBMs as well as the presence and location of bundles, two IFM bands, the presence of defects, and the graphene tangential mode, in concert with endogenous lipids and proteins from the cell. This work demonstrates the possibility of the transient confocal molecular imaging of live cells and tissues using Raman spectroscopy, affording unique photostability and a much greater multiplexing ability than conventional imaging methods.

■ ASSOCIATED CONTENT

Ⓢ Supporting Information

Movies of nanotube uptake acquired by high-speed confocal Raman imaging and supporting figures. This material is available free of charge via the Internet at http://pubs.acs.org.

■ AUTHOR INFORMATION

Corresponding Author

*E-mail: hellerd@mskcc.org.

Notes

The authors declare no competing financial interest.

■ ACKNOWLEDGMENTS

We thank Prof. Peter So for helpful discussions. This work was performed at the MIT Laser Biomedical Research Center and was supported by the NIH National Institute of Biomedical Imaging and Bioengineering, grant P41EB015871-26A1. D.A.H. thanks the Damon Runyon Cancer Research Foundation (DFS-#2050-10) and the Frank A. Howard Fellows Program at Memorial Sloan-Kettering Cancer Center.

■ REFERENCES

(1) Haes, A. J.; Van Duyne, R. P. *J. Am. Chem. Soc.* **2002**, *124*, 10596−10604.
(2) Dresselhaus, M. S.; Dresselhaus, G.; Saito, R.; Jorio, A. *Phys. Rep.* **2005**, *409*, 47−99.
(3) Kam, N. W. S.; O'Connell, M. J.; Wisdom, J. A.; Dai, H. *Proc. Natl. Acad. Sci. U.S.A.* **2005**, *102*, 11600−11605.
(4) Herrero, M. A.; Toma, F. M.; Al-Jamal, K. T.; Kostarelos, K.; Bianco, A.; Da Ros, T.; Bano, F.; Casalis, L.; Scoles, G.; Prato, M. *J. Am. Chem. Soc.* **2010**, *132*, 1731−1731.
(5) Heller, D. A.; Jin, H.; Martinez, B. M.; Patel, D.; Miller, B. M.; Yeung, T. K.; Jena, P. V.; Hobartner, C.; Ha, T.; Silverman, S. K.; Strano, M. S. *Nat. Nanotechnol.* **2009**, *4*, 114−120.
(6) Barone, P. W.; Baik, S.; Heller, D. A.; Strano, M. S. *Nat. Mater.* **2005**, *4*, 86−92.
(7) Allen, B. L.; Kichambare, P. D.; Star, A. *Adv. Mater.* **2007**, *19*, 1439−1451.
(8) Heller, D. A.; Baik, S.; Eurell, T. E.; Strano, M. S. *Adv. Mater.* **2005**, *17*, 2793−2799.
(9) Liu, Z. A.; Li, X. L.; Tabakman, S. M.; Jiang, K. L.; Fan, S. S.; Dai, H. J. *J. Am. Chem. Soc.* **2008**, *130*, 13540−13541.
(10) Keren, S.; Zavaleta, C.; Cheng, Z.; de la Zerda, A.; Gheysens, O.; Gambhir, S. S. *Proc. Natl. Acad. Sci. U.S.A.* **2008**, *105*, 5844−5849.
(11) (a) Jin, H.; Heller, D. A.; Strano, M. S. *Nano Lett.* **2008**, *8*, 1577−1585. (b) Lacerda, L.; Pastorin, G.; Gathercole, D.; Buddle, J.; Prato, M.; Bianco, A.; Kostarelos, K. *Adv. Mater.* **2007**, *19*, 1480−1484.
(12) Kalbacova, M.; Broz, A.; Kromka, A.; Babchenko, O.; Kalbac, M. *Carbon* **2011**, *49*, 2926−2934.
(13) Jorio, A.; Saito, R.; Hafner, J. H.; Lieber, C. M.; Hunter, M.; McClure, T.; Dresselhaus, G.; Dresselhaus, M. S. *Phys. Rev. Lett.* **2001**, *86*, 1118−1121.
(14) Fantini, C.; Jorio, A.; Souza, M.; Saito, R.; Samsonidze, G. G.; Dresselhaus, M. S.; Pimenta, M. A. *Phys. Rev. B* **2005**, *72*, 085446.
(15) Luo, Z. T.; Papadimitrakopoulos, F.; Doorn, S. K. *Phys. Rev. B* **2007**, *75*, 205438.
(16) Fantini, C.; Jorio, A.; Souza, M.; Strano, M. S.; Dresselhaus, M. S.; Pimenta, M. A. *Phys. Rev. Lett.* **2004**, *93*, 147406.
(17) Heller, D. A.; Barone, P. W.; Swanson, J. P.; Mayrhofer, R. M.; Strano, M. S. *J. Phys. Chem. B* **2004**, *108*, 6905−6909.
(18) Puppels, G. J.; de Mul, F. F.; Otto, C.; Greve, J.; Robert-Nicoud, M.; Arndt-Jovin, D. J.; Jovin, T. M. *Nature* **1990**, *347*, 301−303.
(19) Kang, J. W.; Lue, N.; Kong, C. R.; Barman, I.; Dingari, N. C.; Goldfless, S. J.; Niles, J. C.; Dasari, R. R.; Feld, M. S. *Biomed. Opt. Exp.* **2011**, *2*, 2484−2492.
(20) Uzunbajakava, N.; Lenferink, A.; Kraan, Y.; Volokhina, E.; Vrensen, G.; Greve, J.; Otto, C. *Biophys. J.* **2003**, *84*, 3968−3981.
(21) Zheng, M.; Jagota, A.; Semke, E. D.; Diner, B. A.; Mclean, R. S.; Lustig, S. R.; Richardson, R. E.; Tassi, N. G. *Nat. Mater.* **2003**, *2*, 338−342.
(22) Bronikowski, M. J.; Willis, P. A.; Colbert, D. T.; Smith, K. A.; Smalley, R. E. *J. Vac. Sci. Technol., A* **2001**, *19*, 1800−1805.
(23) Jiang, J.; Saito, R.; Gruneis, A.; Chou, S. G.; Samsonidze, G. G.; Jorio, A.; Dresselhaus, G.; Dresselhaus, M. S. *Phys. Rev. B* **2005**, *71*, 205420.